# Journal of Physics:
Condensed Matter

TOP PAPERS 2004
SHOWCASE

Top Papers 2004 Showcase highlights the leading and most frequently downloaded papers, letters and topical reviews to *Journal of Physics: Condensed Matter*, arguably the world's most authoritative source of topical information for condensed matter physicists and materials and surface scientists. *Journal of Physics: Condensed Matter* covers experimental and theoretical studies of the structural, thermal, mechanical, electrical, magnetic and optical properties of condensed matter and is published 50 times per year by Institute of Physics Publishing.
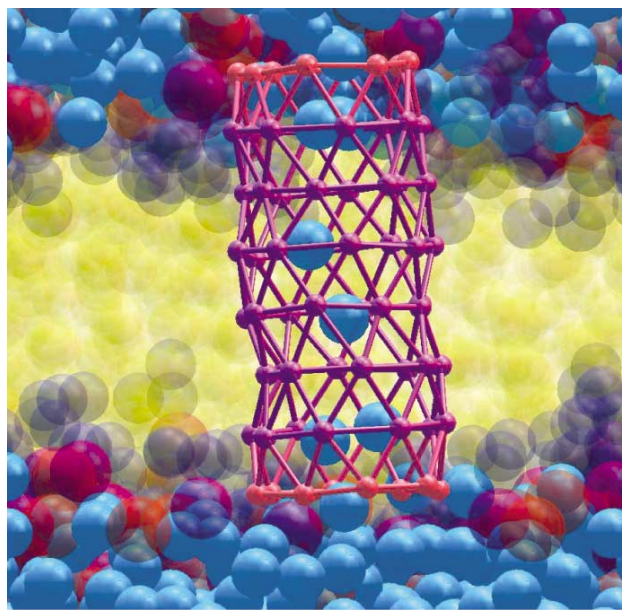
Water transport across a capped nanotube embedded in a lipid bilayer. A snapshot of water (blue) diffusing across the HBTC tube embedded in a CG-DMPC bilayer. The hydrophobic part of the tube is depicted in purple, and the hydrophilic caps in red. The lipid tails (yellow), phosphate unit (purple), choline unit (red), glycerol and ester groups (dark blue) and semitransparent.)

(See page 10)

We welcome papers and submissions from authors who have research interests in these areas. Authors can benefit from rapid receipt-to-publication times, a rising impact factor and a large and growing world wide readership both in print and on-line. On average papers are downloaded on-line over 100 times via our award winning Electronic Journals service. For more information on the submission process and to view the latest published papers visit **www.iop.org/journals/jpcm**

PAPERS
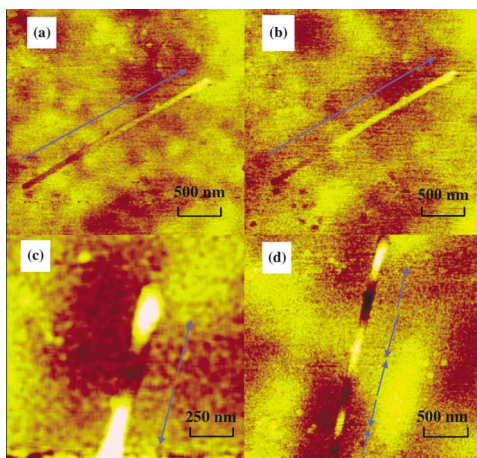
TOPICAL REVIEWS AND SPECIAL ISSUE PAPERS

Inside you will find synopses of all the top papers and reviews listed above, together with details of where to find the full articles ➤➤➤➤

Magnetism in carbon nanotubes

Contact induced magnetism in carbon nanotubes

O Céspedes, M S Ferreira, S Sanvito, M Kociak and J M D Coey

J. Phys.: Condens. Matter 16 No 10 L155-L161

Magnetic force micrographs of a multiwalled nanotube lying on a magnetite substrate obtained in the amplitude mode with a low-moment, permalloy-coated tip.

Diamond and graphite have many outstanding properties, but magnetism is not expected to be very evident in such a light element. There have been reports of weak ferromagnetism in graphite and other forms of carbon due to a magnetic proximity effect. Michael Coey's group at Trinity College Dublin set out to find direct experimental evidence of contact-induced magnetism, and gain some understanding of its origin. Their idea was to place a carbon nanotube in contact with a ferromagnet and measure the spin transfer associated with the alignment of their chemical potentials. The problem of detecting the tiny spin transfer against the huge background magnetic moment of the ferromagnet was resolved by taking a smooth ferromagnetic thin film as a substrate and looking for a stray field around the nanotube. Uniformly magnetized thin films create no stray field, whatever their direction of magnetization, so any observed stray field must arise from the tube.

Tubes were placed on the different substrates, and topographic and magnetic images were recorded by atomic and magnetic force microscopy (AFM/MFM). Magnetic contrast was observed for carbon nanotubes placed on cobalt or magnetite substrates, but was absent on silicon, copper or gold substrates.

The figure shows some images of a carbon nanotube on Fe_3O_4 taken at different scan heights. The magnetic images in figures (a) and (b) show little contrast to the magnetite substrate, and clear bipolar contrast to the nanotube, as expected if it were a single domain magnetized along its length. These images suggest that the tube is aligned with the direction of magnetization of a single, in-plane domain in the substrate. Shape anisotropy of the film ensures that its magnetization lies in-plane, and any weak stray field comes from surface irregularity, ripple domains or Bloch walls. The images in figures (c) and (d) are of the same tube in a slightly different position.

These studies give direct evidence for contact-induced magnetism due to spin-polarized charge transfer at a contact between a ferromagnet and a carbon nanotube with a spin transfer of the order of $0.1\mu_B$ per contact carbon atom, and an induced magnetization of the order of $1\,kA\,m^{-1}$ in multiwalled nanotubes.

This observation of contact-induced magnetism opens a new avenue for implementing spin-electronics at the molecular level, where the current leads can be separated from the electrodes producing spin polarization.

Superconductivity and Electron Correlation in a ternary oxide

Superconductivity in a pyrochlore-related oxide KOs_2O_6

S Yonezawa, Y Muraoka, Y Matsushita and Z Hiroi

J. Phys.: Condens. Matter 16 No 3 L9-L12
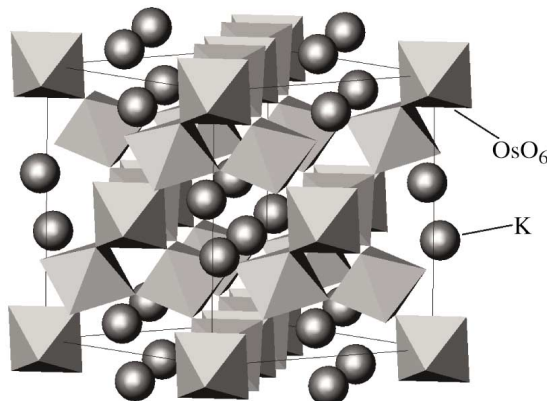
Probable crystal structure for KOs_2O_6. K, Os and O atoms occupy the 8b, 16c and 48f sites in the space group $Fd\bar{3}m$, respectively.

Pyrochlore oxides have a general chemical formula $A_2B_2O_7$ or $A_2B_2O_6O'$, where A is a larger cation and B is a smaller transition metal (TM) cation. Most pyrochlore oxides containing 5d TM elements such as Re, Os and Ir are bad metals. Recently, superconductivity was found for the first time in a pyrochlore oxide in $Cd_2Re_2O_7$ at $Tc = 1$ K. A related pyrochlore oxide $Cd_2Re_2O_7$ undergoes a metal-insulator (MI) transition at 225 K. The major difference between them seems to be the number of d electrons on the B-site cations: Re^{5+} being $5d^2$ and Os^{5+} $5d^3$.

Z Hiroi and co-workers at The University of Tokyo report the discovery of superconductivity in a new ternary phase KOs_2O. Polycrystalline samples were prepared from KO_2 and OsO_2 powders. Resistivity measurements showed a superconducting transition with onset temperature 9.9 K and zero resistivity below 9.0 K. When a magnetic field was applied, the transition curve shifted to lower temperatures systematically. The resistivity above the transition shows a peculiar temperature dependence, which is far from that of a conventional metal. Measurements on a single crystal instead of a polycrystalline pellet are needed to clarify this point. The sample also showed a Meissner effect below 9.6 K. The superconducting volume fraction estimated at 2 K from the zero-field cooling experiment is about 80%, which is large enough to constitute bulk superconductivity.

The authors believe that an interesting physical process is involved in this compound on the basis of electron correlations near the MI transition as well as frustration on the pyrochlore lattice.

See also a recent review by P W Anderson et al.

The physics behind high-temperature superconducting cuprates: the 'plain vanilla' version of RVB

P W Anderson, P A Lee, M Randeria, T M Rice, N Trivedi and F C Zhang

J. Phys.: Condens. Matter 16 No 24 R755-R769

In this review, Anderson and co-workers revisit the RVB theory using the 'renormalized mean field theory'. They observe that it is able to explain the existence of the pseudogap, properties of nodal quasiparticles and approximate spin-charge separation, the latter leading to large renormalizations of the Drude weight and superfluid density. Finally, they remark that superexchange, and not phonons, is responsible for d-wave superconductivity in the cuprates.

Network formation in soft-solid composites

The origin of network formation in colloid-liquid crystal composites

Doris Vollmer, Gerald Hinze, Wilson C K Poon, Julie Cleaver and Michael E Cates

J. Phys.: Condens. Matter 16 L227-L233
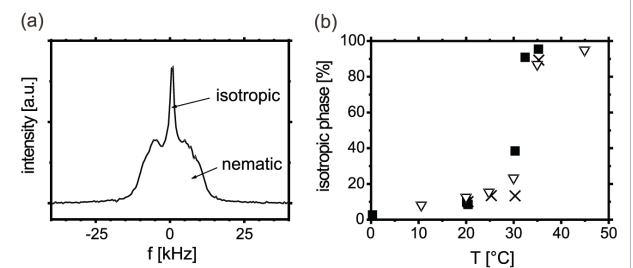
(a) A ^1H NMR solid echo spectrum, taken at 30 °C (particle size: R = 430 nm). (b) The temperature dependence of the fraction of the isotropic phase for different particle sizes. ■: R = 120 nm; ▽: R = 430 nm; ✕: R = 780 nm. Weight fraction of colloids: 15%.

Network formation in soft solids affects the way they respond to stress and many other properties. In mixed liquid crystal / colloid systems, the tendency of liquid crystal molecules to align will affect phase structures. What has been less obvious is the role of small alkane impurity molecules, which prove to "tune" the kinetics of phase separation.

When liquid crystals are mixed with colloids, the particles disturb the long-range orientational order the liquid crystal molecules can adopt. Consequently, the orientational elasticity of the nematic liquid crystals expels the colloids, so typically the suspension phase separates macroscopically into an almost pure liquid crystalline phase coexisting with a phase rich in colloids. However, long-lived non-macrophase-separatedmorphologies have also been observed.

Wilson Poon and co-workers at Edinburgh and Mainz have investigated network formation by comparing detailed rheological, nuclear magnetic resonance (NMR) and calorimetric measurements. They studied suspensions of 4-*n*-pentyl-4′-cyanobiphenyl (5CB) and polymethylmethacrylate particles (PMMA) with nominal radii of 120, 370 and 780 nm, sterically stabilized by chemically grafted poly-12-hydroxy stearic acid of ≈15 nm thickness. The results challenge aspects of the data and theoretical explanations in the current literature, and reveal a crucial role played by alkane impurities.

Rheological data suggest that, contrary to previous expectation, network formation is possible with particles over a broad range of sizes. Only little dependence on particle size is observed. NMR data indicate the presence of a significant fraction of isotropic material down to 10 K below the bulk nematic transition of the liquid crystal. Calorimetric findings suggest that small amounts of alkane impurities, carried originally by the dispersed particles, are present. These molecules act as a second solvent. They play a crucial role in 'tuning' the kinetics of phase separation to allow network formation by (i) opening up a biphasic region and (ii) wetting the particles with a layer of isotropic material.

Unexpected atom exchange in surface diffusion

Novel exchange mechanisms in the surface diffusion of oxides

Duncan J Harris, Mikhail Yu Lavrentiev, John H Harding, Neil L Allan and John A Purton
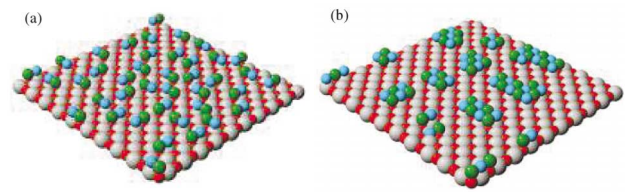
Evolution of BaO islands on the (100) surface of BaO. (a) Starting configuration; (b) after 380 ns simulation at 1000 K.

Usually, one expects surface diffusion to occur simply by adatoms moving around on top of the surface atoms. Surprisingly, in some oxides, the diffusing species move most rapidly by exchanging with substrate atoms. This behaviour, unexpected in oxides, showed up through new methods of simulation. Work by John Harding (UCL) and Neil Allen (Bristol) and colleagues shows the importance of exchange mechanisms in surface diffusion on oxides. Simulation of diffusion in simple ceramics presents particular problems because energy barriers are often high, so it is impossible to run molecular dynamics simulations for long enough to obtain adequate statistics. Temperature accelerated dynamics (TAD) uses simulations performed at high temperature to calculate the evolution of systems at a lower temperature of interest.

The authors have simulated the diffusion of BaO molecules along the (100) surface of a BaO substrate. The TAD calculations clearly show that the diffusion mechanism with the lowest barrier involves exchange with surface ions.

They have also calculated the mean formation time of islands on the surface, starting from a random distribution of molecules. As the simulation proceeds, randomly moving pairs meet and create initial clusters, which cannot move; the proto-steps so produced attract molecules in turn, resulting in the spontaneous creation of islands. Including the exchange mechanism drastically accelerates island formation. The evolution of the islands is shown in the figure.

Molecular beam epitaxy is being used to create layered structures of ferroelectric, ferromagnetic and dielectric oxides. The question of whether the exchange mechanism is still active when a molecule of one oxide diffuses on a different oxide substrate is of fundamental importance for creating sharp interfaces in such structures. The authors have performed calculations using a BaO molecule on the (100) SrO surface and SrO on the (100) BaO surface. The large size of the barium ion, relative to the strontium ion, prevents embedding of the Ba ion into the SrO surface, whereas the Sr ion readily exchanges with a surface layer barium ion. In this case the activation energy is about 0.6 eV. The existence of this low-energy mechanism suggests that, in some cases at least, ionic materials cannot be grown on a substrate with a similar structure without significant intermixing.

The authors have shown the importance of exchange mechanisms in a variety of surface diffusion processes in simple oxides. The mixing effect inherent in such a process means that the possibility of these mechanisms must be considered when attempting to build oxide nanostructures and multilayers.

Surface recrystallization by electrons

Electron-stimulated athermal surface recrystallization of Si(100)

Tetsuya Narushima, Masahiro Kitajima and Kazushi Miki
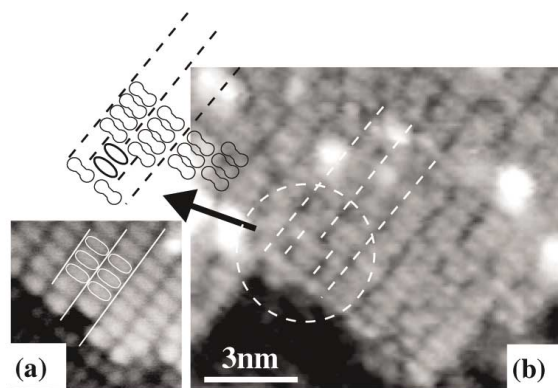
Detailed comparison between (a) a typical thermally annealed surface and (b) an electron-irradiated surface after ion bombardment. Out-of-phase dimers are seen in the broken circle.

Electronic excitation is a remarkably effective tool for controlled modification of materials. Even low-energy electron beams, typically under 5000 eV, routinely used to investigate the structural and chemical properties of surfaces, can cause structural changes. Tetsuya Narushima and colleagues at National Institute for Materials Science have found a more surprising result: complete restoration of the disorder-induced surface stress of Si(100) occurs for electrons of low energies 3.75-40 eV. Upon irradiating the disordered Si surface, disorder-induced compressive stress completely relaxed. The stress relaxation was found to depend only on the number of irradiated electrons and was independent of the total energy deposition, indicating an underlying mechanism that is athermal. They suggest that there is a threshold around 40-90 eV (in the case of Si) between athermal and thermal electron-surface atom interaction processes in the surface layer. At energies below the threshold, the electrons can heal the damage, for example, caused by low-energy Ar+ ions.

In a recent letter, Narushima et al show using scanning tunneling microscopy (STM) that the origin of the athermal surface stress relaxation is recrystallization of the surface atoms. In general, higher-energetic particles are expected to penetrate deeper inside materials, but electrons with extremely low kinetic energy ≪70 eV can penetrate to unusual depths because they cannot lose energy via any energy loss process. Higher-energy electron irradiation (> 90 eV) induces surface defects in the Si surface by electron excitation due to the cascade of inelastic scattering events. Narushima's extremely low-energy electron irradiation achieves restoration of a destroyed structure. A plausible mechanism of the athermal restoration observed is ionization-enhanced diffusion via the charge state transition of defects where no energy loss occurs. In defective Si, electron irradiation promotes athermal diffusion of defects. Such a charge state transition mechanism may occur on the Si surface. Some traces of the athermal restoration on the surface structure could be observed, such as a slightly pairing (1×1) structure and an absence of buckled dimers and out-of-phase dimerization features derived from the athermal process of electron irradiation. In demonstrating that surfaces can have the capacity of self-healing, these results suggest new opportunities for atomic-scale surface engineering.

Non-linear response to ultra-short laser pulses

Response theory for time-resolved second-harmonic generation and two-photon photoemission

C Timm and K H Bennemann
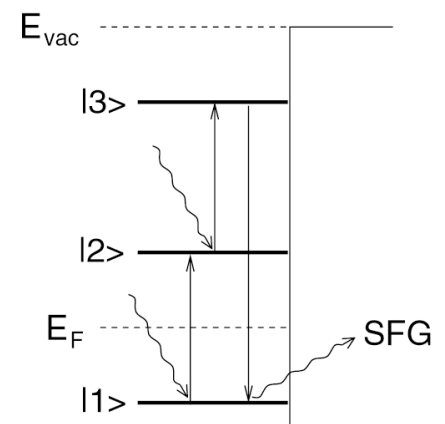
A simplified representation of sum-frequency generation (SFG). E_F is the Fermi energy and E_{vac} is the vacuum energy. In SFG two photons of frequencies ω_1 and ω_2 are absorbed by electrons in states $|1>$ and $|2>$ and a single photon of frequency $\omega_1 + \omega_2$ is emitted due to the electronic transition $|3> \to |1>$. The two photons may be provided by one or two laser pulses. Note that whether the two photons are predominantly absorbed at nearly the same time or with some delay depends on the shape and width of the pulse(s).

It is now possible to create ultrashort (a few femtoseconds) laser pulses, whose duration is similar to the relaxation times of excited electrons and collective excitations in solids. These enable non-equilibrium physics of condensed matter systems to be studied using nonlinear techniques such as time-resolved sum frequency generation (SFG) and two-photon photoemission (2PPE).

A recent paper by Carsten Timm and Karl Bennemann of Free University Berlin presents a unified response theory for the time-resolved second-harmonic generation (SHG) and 2PPE and derives the dependence of the SFG light intensity and the 2PPE photoelectron yield on the time dependence of the exciting laser field. The theory does not rely on any assumption about the time or frequency dependence of the exciting laser pulses. The paper discusses metals but the response theory can be applied to semiconductors and insulators as well.

They study a simple tight-binding model of a metal to show that the theory gives reasonable numerical results and to illustrate effects important for the understanding of SFG and 2PPE. They show how relaxation rates and detuning affect the interference patterns in single-colour pump-probe SHG and 2PPE experiments: the lifetime in the intermediate states and their detuning with respect to the photon energy lead to a similar narrowing of the interference patterns. The effect of detuning must be taken into account in order to extract meaningful lifetimes from such experiments. Also, in particular in SHG the measured relaxation rate is a weighted average over the relaxation rates of many excited states. Furthermore, the weights in this average change with the pump-probe delay. Thus different rates govern the decay of the interference pattern depending on the pump-probe delay-the decay is not simply exponential.

See also a review by Bennemann

Ultrafast dynamics in solids

K H Bennemann

This review analyses the ultrafast response of metals and semiconductors to electronic excitations.

Simulation of highly disordered solids

Simulation of mineral solid solutions at zero and high pressure using lattice statics, lattice dynamics and Monte Carlo methods

I T Todorov, N L Allan, M Yu Lavrentiev, C L Freeman, C E Mohn and J A Purton

J. Phys.: Condens. Matter 16 S2751-S277
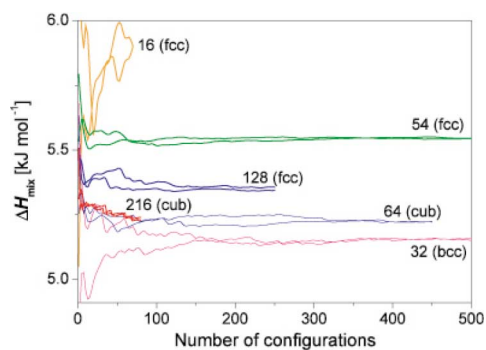
Calculated values of $\triangle H_{mix}$ (kJ mol^{-1}) for a 50/50 MnO-MgO composition at 1000 K as a function of supercell size and number of configurations. The number attached to each curve denotes the total number of atoms in each supercell.

Grossly disordered minerals and many oxides of major practical importance, such as oxide nuclear fuels, present major theoretical challenges. These systems may contain large numbers of defects, or may be non-ideal solid solutions. Neil Allen (Bristol) and colleagues discuss two practical multi-configurational ways to handle such systems with finite impurity or defect concentrations, far from the dilute limit.

The first builds on a highly efficient method for the fully dynamic structure optimization of large unit cells which uses lattice statics and quasiharmonic lattice dynamics (QLD). The accurate calculation of the free energy via QLD is quick and computationally efficient and does not resort to lengthy thermodynamic integration. The full set of free energy first derivatives is calculated analytically and a minimization of the free energy with respect to all structural variables for large unit cells is possible. Here this technique is extended to evaluate the *free energies* of solid solutions (including $\triangle H_{mix}$, $\triangle S_{mix}$) and phase diagrams at *any* pressure. This is achieved by forming a thermodynamic average of the free energies of a number of configurations. Strategies for generating a suitable set of configurations are discussed. We compare results obtained by random generation with those obtained using radial distribution functions or explicit symmetry arguments to obtain approximate or exact weightings respectively for individual configurations.

The second technique is the well-known Monte Carlo method, extended in such a way that *both* the atomic configuration *and* the atomic coordinates of all the atoms are changed. This approach is called Monte Carlo exchange (MCX). While absolute values of the free energy cannot be obtained readily from Monte Carlo simulations, the semigrand canonical ensemble provides a convenient route to accurate chemical potential *differences* accurately and hence the phase diagram.

Both methods are readily applied to high pressures and elevated temperatures without the need for any new parametrization. Agreement between the two techniques is better at high pressures where anharmonic terms are smaller. The authors compare in detail the use of each technique for properties such as enthalpies, entropies, volume and free energies of mixing at zero and high pressure and thus calculation of the phase diagram. They assess the vibrational contributions to these quantities and compare results with those in the dilute limit. The techniques are illustrated throughout using MnO-MgO and should be readily applicable to more complicated systems.

Glass transition of polymer films

Glass transition temperatures of polymer thin films monitored by Raman scattering

H Liem, J Cabanillas-Gonzalez, P Etchegoin and D D C Bradley

J. Phys.: Condens. Matter 16 721-728
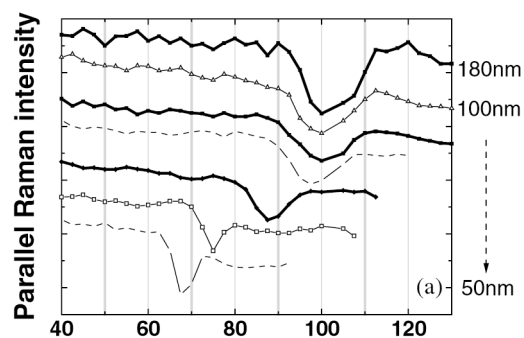
Parallel Raman intensity (I$\parallel$) as a function of T of polystyrene for different film thicknesses going from 180 to 50 nm. A distinct crossover is observed below a specific thickness, which depends on the molecular weight.

Donal Bradley's group at Imperial College London have developed a new method for monitoring the glass transition in polymer thin films, which is of technological importance in polymer devices and an interesting problem of fundamental physics. Below the glass transition the polymer behaves as a hard disordered solid with a microscopic glassy structure, while above it the polymer becomes rubber-like and comparatively softer.

It is known that the effective glass transition in thin films depends strongly on the film thickness and the interfacial interactions. The glass transition temperature of a thin polystyrene film on a Si substrate was found to be depressed by ~20°C whereas in a free-standing film with the same thickness it was depressed by ~70 °C, clearly showing the role of interfacial interactions.

It has been suggested that the boundary of the film has a surface layer of finite thickness with an increased mobility, producing a lower Tg. This high-mobility layer increases as the temperature approaches the bulk Tg upon heating. The origin of the increased mobility of the polymer chains at the surface layer is still not clear.

Previously, Brillouin scattering has been used to monitor Tg, but Bradley introduced the use of confocal Raman spectroscopy. Experiments were performed on free-standing polystyrene films with varying thickness as a model study to validate the technique. Excellent agreement with previous determinations of Tg by other techniques was found.

The technique offers further possibilities, which are not fully exploited in the case of polystyrene owing to its simple nature. As pointed out before, polarized scattering in polystyrene gives essentially the same qualitative information for both I$\parallel$ and I$\perp$, but this is not necessarily the case in more complex polymers that may display molecular order at the surfaces. The authors have found evidence of this in thin films of a conjugated polymer. They also found evidence of a crossover in which two glass transitions are observed if $R_{EE} < d$ (R_{EE} = polymer chain length and d = thickness of the film) but only a single transition is observed if $R_{EE} > d$. A simple interpretation of this is that, for $R_{EE} > d$, the distinction between the surface and the bulk of the film becomes impossible to make and a single transition is expected accordingly.
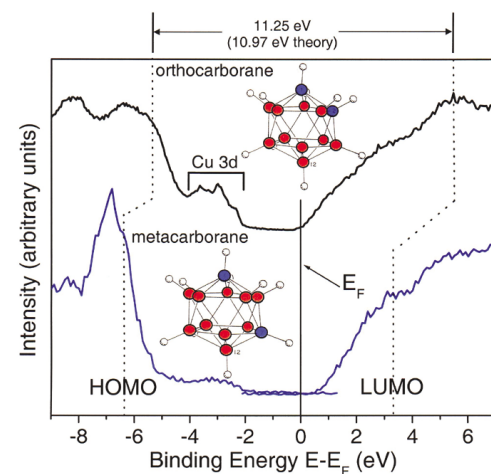
All these results are part of a more comprehensive study of glass transitions in conjugated polymer thin films which is underway.

Making a diode from isomers

The heteroisomeric diode

Anthony N Caruso, Ravi B Billa, Snjezana Balaz, Jennifer I Brand and P A Dowben

J. Phys.: Condens. Matter 16 L139-L146

The HOMO-LUMO gap of orthocarborane ($C_2B_{10}H_{12}$) (top) and metacarborane ($C_2B_{10}H_{12}$) (bottom). Shown are the combined photoemission (left) and inverse photoemission (right) spectra of the molecular thin films on gold and copper for metacarborane and orthocarborane respectively. The highest occupied molecular orbital (HOMO) and the lowest unoccupied molecular orbital (LUMO) are identified from detailed coverage-dependent studies and compared with the theoretical expectations for the isolated molecule. Blue atoms are carbon and red are boron. The Fermi level is closer to the binding energy of the HOMO for orthocarborane and closer to the LUMO for metacarborane.

Semiconductor diodes are based on a junction between p- and n-type materials. They are usually either heterojunctions (made of two different semiconductors) or homojunctions (a single semiconductor doped to form p-type and n-type regions). The heteroisomeric diode is a new type of diode formed between two polytypes of the same material where one polytype is effectively p-type and the other n-type. This is possible if the semiconductor can exist in different polytypes (i.e. different atomic arrangement with the same chemical composition).

Peter Dowben's group at University of Nebraska Lincoln have made heteroisomeric diodes by chemical vapour deposition (CVD) from two different isomers of *closo*-dicarbadodecaborane ($C_2B_{10}H_{12}$) - which tend to form p- and n-type semiconducting boron carbide respectively. These carborane heteroisomer diodes have many advantages over the previously fabricated heterojunction and homojunction diodes. The isotope ^{10}B has a large neutron capture cross-section, so diodes with vastly improved sensitivity can be made by using 100% ^{10}B (its natural abundance is about 20%). This can be achieved efficiently via ^{10}B enrichment of the carborane source molecules used for CVD. Furthermore, since the heteroisomeric diodes are formed without transition metal dopants, activatible transition metals can be eliminated, leading to increased reliability and fewer false positive signals.

Neutron detection efficiencies of these new diodes have yet to be measured, and they have not, as yet, exhibited the insensitivity to high temperature found with the silicon carbide/boron carbide heterojunction and the boron carbide homojunction diodes. Nonetheless, the heteroisomeric diodes packaged in organic polymers (that also act as a neutron moderator) are more efficient and subject to fewer false positives than some recent schemes for detecting fissile materials. Even without isotopic enrichment, since the depletion regions and both sides of the p-n junction contain a boron-rich semiconductor, the heteroisomeric diodes represent a potentially far more efficient (and hence sensitive) solid state neutron detector than any conversion layer or heterojunction layer device.

Anisotropy in magnetic semiconductors

Magnetic anisotropy and domain structure in carrier-controlled ferromagnetic semiconductors
Tomasz Dietl
J. Phys.: Condens. Matter 16 S5471-S5479
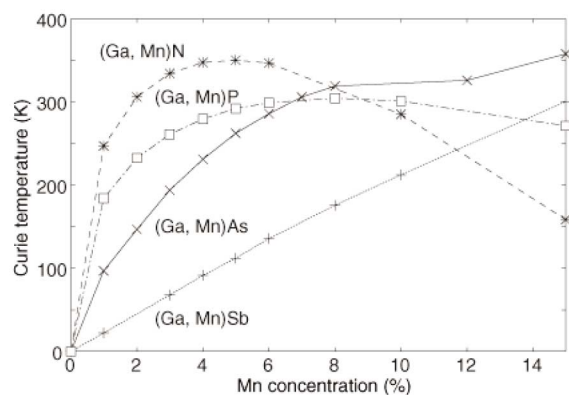
Curie temperatures of (Ga, Mn)N, (Ga, Mn)P, (Ga, Mn)As and (Ga, Mn)Sb calculated from first principles in the mean field approximation. [from Exchange interactions in diluted magnetic semiconductors, K Sato, P H Dederichs, H Katayama-Yoshida and J Kudrnovsk_, J. Phys.: Condens. Matter 16 S5491-S5497]

There is an intense search for room-temperature spintronic semiconductor materials. Much effort has been devoted to understanding the nature of carrier-controlled ferromagnetism in tetrahedrally coordinated diluted magnetic semiconductors (DMS), such as (Ga, Mn)As. A theory based on Zener's model of ferromagnetism, the Ginzburg-Landau approach to the phase transitions, and the Kohn-Luttinger *kp* theory of semiconductors accounts for the magnetic properties of Mn-doped GaAs, InAs, GaSb, and InSb as well as in p-CdTe, p-ZnTe, and Ge, assuming that the long-range ferromagnetic interactions between the localized spins are mediated by the holes in the weakly perturbed valence band. The understanding of (III, Mn)As alloys has provided a basis for the development of novel methods enabling magnetization manipulation and switching.

Tomasz Dietl of the Polish Academy of Sciences reviews the experimental situation and theoretical modelling of the micromagnetic properties of (Ga, Mn)As and related compounds. Interestingly, despite much lower spin and carrier concentrations compared with ferromagnetic metals, these materials exhibit excellent micromagnetic characteristics, including well defined magnetic anisotropy and large and ferromagnetic domains separated by usually straight-line domain walls.

The Zener p-d model explains quantitatively the effect of strain on the easy axis direction as well as predicting correctly the presence of the reorientation transition, observed as a function of hole concentration and temperature. Possible suggestions to explain the existence of in-plane uniaxial magnetocrystalline anisotropy are put forward. Finally, magnetic stiffness computed within the same model of ferromagnetism is presented, and is shown to explain the domain width in perpendicular films. It is emphasized that a rather large magnitude of the stiffness accounts for both the excellent micromagnetic properties of ferromagnetic (III, Mn)V films and the quantitative applicability of the mean-field approximation to these materials.

Energy landscape of glassy polystyrene

A study of the deep structure of the energy landscape of glassy polystyrene: the exponential distribution of the energy barriers revealed by high-field electron spin resonance spectroscopy
V Bercu M Martinelli, C A Massa, L A Pardi and D Leporini
J. Phys.: Condens. Matter 16 L479-L488
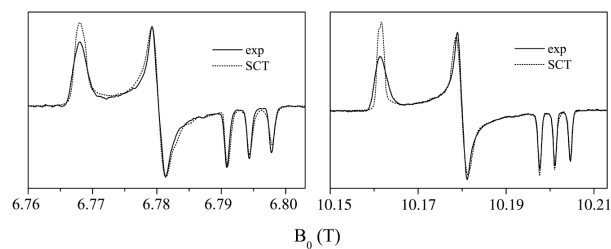
The ESR line shapes at 190 GHz (left) and 285 GHz (right) of TEMPO in PS at 50 K. The magnetic parameters are: $g_x = 2.009\ 94 \pm 3 \times 10^{-5}$, $g_y = 2.006\ 28 \pm 3 \times 10^{-5}$, $g_z = 2.002\ 12 \pm 3 \times 10^{-5}$, $A_x (mT) = 0.62 \pm 0.02$, $A_y (mT) = 0.70 \pm 0.02$, $A_z (mT) = 3.40 \pm 0.02$. The superimposed dashed curves are best fits according to the SCT model, with $\tau_{SCT} = 25$ ns (190 GHz) and $\tau_{SCT} = 19$ ns (285 GHz). The jump angle $\phi = 60°$. The theoretical lineshapes were convoluted by a Gaussian with width $w = 0.15$ mT to account for the inhomogeneous broadening.

Solid glassy dynamics is currently an active field of study. At temperatures well below the glass transition temperature T_g (so the ageing effect can be ignored) but high enough that the tunnelling effects governing the low-temperature anomalies of glasses can be ignored, the dynamics is thermally activated in the substructures of the minima of the energy landscape accounting for various subtle degrees of freedom. In a glass the temperature dependence of the energy barrier distribution $g(E)$ is only weakly temperature dependent.

The shape of the energy barrier distribution $g(E)$ in glasses has been extensively investigated by experiments, theories and simulations. It is usually found to be either Gaussian or exponential. A convolution of these two distributions as well as the truncated Levy flight, i.e. a power law with exponential cut-off, resembling a stretched exponential have also been considered.

D Leporini and co-workers from Pisa have studied the reorientation of one small paramagnetic molecule (spin probe) in glassy polystyrene by high-field electron spin resonance spectroscopy at two different Larmor frequencies (190 and 285 GHz). They found unambiguous evidence for an exponential distribution of the energy barriers for the rotational motion of the spin probe at both 240 and 270 K. The same shape for the distribution of the energy barriers of polystyrene was evidenced by the master curves provided by previous mechanical and light scattering studies. The breadth of the energy barrier distribution of the spin probe is in the range of the estimates of the breadth of the polystyrene energy barrier distribution. The evidence that the deep structure of the energy landscape of polystyrene exhibits the exponential shape of the energy barrier distribution agrees with the results from extreme-value statistics previously found by Bouchaud and co-workers.

Charged critical fluctuations in an oxide superconductor

Evidence for charged critical fluctuations in underdoped $YBa_2Cu_3O_{7-\delta}$
T Schneider, R Khasanov, K Conder, E Pomjakushina, R Bruetsch and H Keller
J. Phys.: Condens. Matter 16 L437-L442
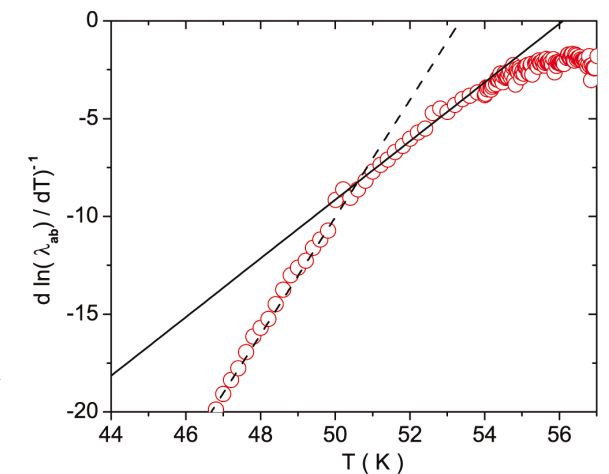
$(d \ln \lambda_{ab}/dT)^{-1}$ with λ_{ab} in μm versus T for $YBa_2Cu_3O_{6.59}$. The straight line with slope $1/\nu \simeq 3/2$ corresponds to charged criticality with $T_c = 56.1$ K, while the dashed line indicates the intermediate 3D XY critical behaviour with slope $2/\nu \simeq 3$.

Close to the critical temperature T_c of the normal-superconductor transition, order parameter fluctuations dominate the critical properties. For strongly type I materials the coupling of the order parameter to transverse gauge field fluctuations is expected to render the transition first order, whereas strongly type II materials should exhibit a continuous phase transition, and sufficiently close to T_c the charge of the order parameter is relevant. However, in cuprate superconductors within the fluctuation-dominated regime, the region close to T_c, where the system crosses over to the regime of charged fluctuations, turns out to be too narrow to access. For instance, optimally doped $YBa_2Cu_3O_{7-\delta}$, while possessing an extended regime of critical fluctuations, is too strongly type II to observe charged critical fluctuations. However, underdoped cuprates could open a window onto this new regime because κ is expected to become rather small. Noting that T_c decreases on approaching the underdoped limit, sufficiently homogeneous and underdoped cuprates appear to be potential candidates to observe charged critical behaviour.

T Schneider and co-workers in Zürich report and analyse in-plane penetration depth measurements of underdoped $YBa_2Cu_3O_{7-\delta}$ to explore the evidence for this new critical behaviour. These measurements provide consistent evidence for the charged critical behaviour of the superconductor-normal state transition in type II superconductors ($\kappa > 1/\sqrt{2}$). Since the effective dimensionless charge $\tilde{e} = 1/\kappa$ scales as $T_c^{-1/2}$ this new critical behaviour should be observable in suitably underdoped cuprates. In this regime the crossover upon approaching T_c is thus to the charged critical regime, while near optimum doping it is to the critical regime of a weakly charged superfluid where the fluctuations of the order parameter are essentially those of an uncharged superfluid. Furthermore, there is the inhomogeneity induced finite size effect which renders the asymptotic critical regime and with that the charged regime of nearly optimally doped samples difficult to attain

Unusual magnetic structures in Gd₂Ti₂O₇

Phase transitions, partial disorder and multi-k structures in $Gd_2Ti_2O_7$
J R Stewart, G Ehlers, A S Wills, S T Bramwell and J S Gardner
J. Phys.: Condens. Matter 16 L321-L326
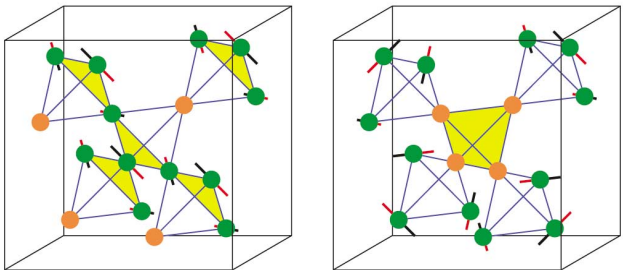
*Comparison of (left) the 1-*k *structure and (right) its 4-k variant. In each structure the four Gd^{3+} ions coloured orange are shown as carrying no thermally averaged moment. The phase transition at T′ = 0.7 K involves weak ordering of these four spins and a small canting of the remaining spins away from the positions shown. At T << 0.7 K, only these ions carry a disordered spin component.*

Magnetic oxides show an enormous variety of spin structures, magnetic phase transitions, and phenomena such as frustration. They pose challenges to theory and experiment, and force new thinking about cooperative phenomena. Ross Stewart of ILL, Grenoble, with co-authors from Oak Ridge, UCL and NIST, have studied the geometrically frustrated antiferromagnet $Gd_2Ti_2O_7$, which exhibits particularly interesting and complex magnetic behaviour. Magnetic ordering commences at T_N = 1.1 K and there is a further magnetic phase transition at $T′ = 0.7$ K.

The technique of neutron diffraction enables the direct determination of complex magnetic structures, but it can be ambiguous when applied to systems of high symmetry, where the problem of 'multi-k' structures arises. Alternative structures, described by one or several symmetry-related propagation vectors k, give identical diffraction patterns as a result of orientational averaging in powders or 'k-domain' formation in single crystals. To distinguish such structures is difficult.

The 1-k and 4-k structures of $Gd_2Ti_2O_7$ are shown in the figure. In the 4-k structure, all spins (in both sets) are perpendicular to the *local* trigonal ‹111› axes (that connect the vertices of the tetrahedra to their centres), while in the 1-k structure the spins are perpendicular to a single *global* [111] crystallographic direction. However, the disordered spin components—which are associated with *only* the weakly ordered set—have a completely different spatial distribution in the 1-k and 4-k structures. In the 1-k structure, nearest neighbour disordered spin components are separated by 7.2Å, while in the 4-k structure they are separated by 3.6 Å. The magnetic diffuse neutron scattering from the two structures must therefore be substantially different.

Between $T′$ and T_N the structure is partly ordered, as previously reported. Below $T′$ the remaining spins order, but only weakly. The magnetic structure in this temperature range is shown to be a 4-k structure, closely related to the 1-k structure previously suggested. The 4-k and 1-k variants of the structure are distinguished by analysis of the diffuse scattering, which represents a new method of solving the 'multi-k' problem of magnetic structure determination.

Ferroelectric nano-capacitors

Intrinsic dielectric response in ferroelectric nano-capacitors
M M Saad, P Baxter, R M Bowman, J M Gregg, F D Morrison and J F Scott
J. Phys.: Condens. Matter 16 L451-L456
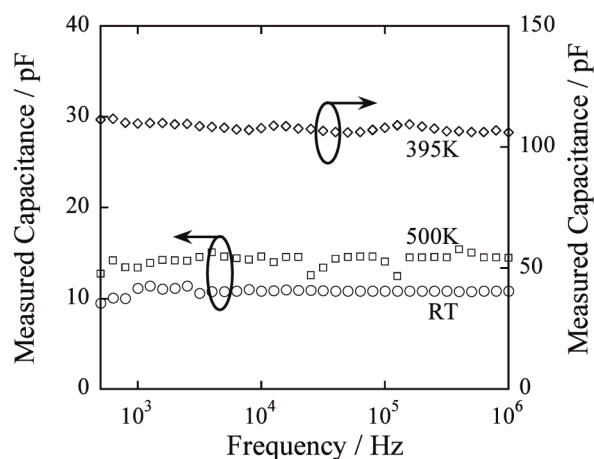
The frequency dependence of the capacitance measured at three different temperatures for thin $BaTiO_3$ lamellae. All lamellae investigated showed the distinct lack of spectral dependence illustrated here. Strong temperature dependence is, however, evident.

Ferroelectric perovskite oxides are key materials in random access memory (RAM) technology, but the origins of changes in functional properties between thin film and bulk remain unresolved. Ferroelectric thin films show a significant broadening of the Curie anomaly (peak in dielectric constant with respect to temperature) as films are made thinner. The broadening of the dielectric peak is associated with an apparent change in the nature of the paraelectric-ferroelectric phase transition from first to second order.

Jim Scott (Cambridge) with co-workers in Belfast have performed measurements on 'free-standing' single-crystal barium titanate capacitors with thickness down to 75 nm, which show a dielectric response typical of large single crystals rather than conventional thin films, with no broadening or temperature shift of the dielectric peak or loss tangent. They observed peak dielectric constants of ~25 000 and Curie-Weiss analysis demonstrated first order transformation behaviour. This is in dramatic contrast to results on conventionally deposited thin film capacitor heterostructures, which show large dielectric peak broadening and temperature shifts, as well as an apparent change in the nature of the paraelectric-ferroelectric transition from first to second order. Their data are compatible with a recent model by Bratkovsky and Levanyuk, which attributes dielectric peak broadening to gradient terms that will exist in any thin film capacitor heterostructure. The observed recovery of first order transformation behaviour is consistent with the absence of significant substrate clamping in our experiment, as modelled by Pertsev et al, and illustrates that the second order behaviour seen in conventionally deposited thin films cannot be attributed to the effects of reduced dimensionality in the system, nor to the influence of an intrinsic universal interfacial capacitance associated with the electrode-ferroelectric interface. Rather, the influence of homogeneous strain through strain coupling to a substrate, or gradient terms associated with chemical, defect or strain gradients, are the primary suspects.

Heat dissipation in nanostructures

Open-boundary Ehrenfest molecular dynamics: towards a model of current induced heating in nanowires
Andrew P Horsfield, D R Bowler and A J Fisher
J. Phys.: Condens. Matter 16 No 7 L65-L72
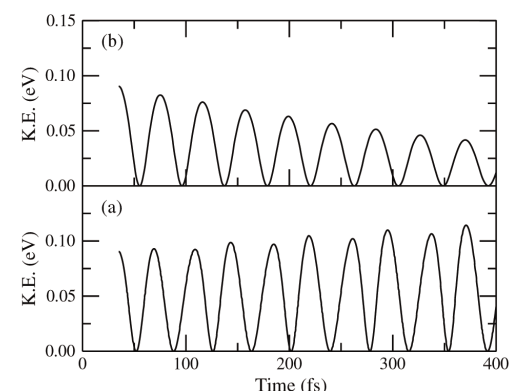
The variation of the ionic kinetic energy of the mobile atom with time for a bias of (a) 0.1 V and (b) 1.0 V. The device contains 3 atoms, and the leads 16 atoms. The initial temperature is about 600 K.

Much of nanotechnology is driven by demands for smaller, faster and more robust devices. Yet reducing sizes brings problems, one being heat dissipation in nanoelectronic devices. To calculate heat dissipation in a nanoscale device, where most standard assumptions fail, is the challenge addressed by Andrew Horsfield, David Bowler and Andrew Fisher at University College, London. They developed a time-dependent method based on the single-particle electron density matrix that allows the electronic and ionic degrees of freedom to be modelled within the Ehrenfest approximation in the presence of open boundaries. It describes a practical implementation using tight binding, and uses it to investigate steady-state conduction through a single-atom device and to perform molecular dynamics. It is found that in the Ehrenfest approximation an electric current allows both ionic heating and cooling to take place, depending on the bias.

To monitor ionic heating the authors follow the evolution of the kinetic energy with time (see figure). For a small bias (0.1 V) the ionic kinetic energy decays with time (cooling), while for a large bias (1.0 V) the kinetic energy increases (heating). The energy ($\hbar\omega$) associated with the vibrational frequency of the ion is 0.055 eV, and equals the Born-Oppenheimer surface separation for allowed transitions. Hence the change in bias increases approximately tenfold the number of possible heating transitions, producing the observed changed behaviour. This method is thus able to calculate some non-adiabatic effects of current flow. However, the amount of heating that is observed for a bias of 1 V is much less than would be expected from quantum perturbation theory. This is the subject of ongoing work by the authors.

See also a recent topical review by David Bowler.

Atomic-scale nanowires: physical and electronic structure
D R Bowler
J. Phys.: Condens. Matter 16 R721-R754

The technology to build and study nanowires with sizes ranging from individual atoms to tens of nanometres has been developing rapidly over the last few years. This review surveys the motivation behind these developments, and summarizes the basics behind quantized conduction. It describes several of the different experimental techniques and materials systems used in the creation of nanowires, and the range of theoretical methods developed both for examining open systems (especially their conduction properties) and for modelling large systems. It presents various noteworthy example results from the field, and concludes with a look at future directions.

Multiple spin-relaxation in CMR materials

The origin of multiple spin-relaxation channels below the metal-insulator transition in ferromagnetic colossal magnetoresistance (CMR) manganites

R H Heffner, D E MacLaughlin, G J Nieuwenhuys and J E Sonier
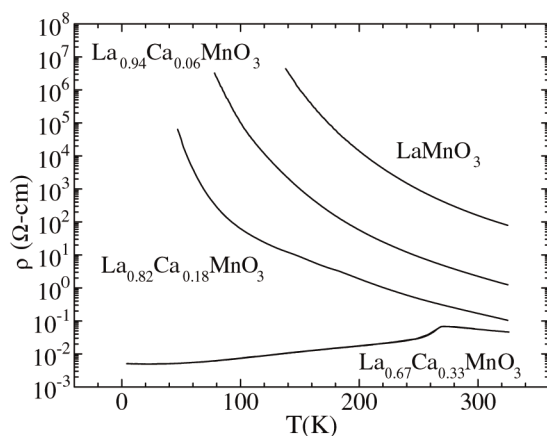
Temperature dependence of the resistivity for class I La$_{1-x}$Ca$_x$MnO$_3$ for x = 0.0, 0.06, 0.18 and 0.33.

Perovskite-structured Mn-based materials show a range of interesting properties that can be controlled by doping with divalent alkaline earth elements. Of particular interest is 'colossal magnetoresistance' (CMR): a reduction (×10) in resistance occurs near the metal-insulator transition temperature T_{MI} when a magnetic field of a few tesla is applied. CMR materials are under intense investigation for their possible use in spintronics devices, for which spin relaxation is an imprtant issue.

Bob Heffner (Los Alamos) and co-workers have performed a series of muon spin relaxation (μSR) experiments on perovskite manganites in the La$_{1-x}$Ca$_x$MnO$_3$ series. Their main focus was the observation of two distinct Mn relaxation channels in ferromagnetic CMR materials. Conventional homogeneous ferromagnets exhibit only a single relaxation channel above and below the Curie temperature T_C. As La$_{1-x}$Ca$_x$MnO$_3$ ferromagnets near optimal doping had been believed to reach a homogeneous state just a few degrees below T_C due to the long-range transport of the doped holes that give rise to a metallic state, the initial observation of multiple relaxation channels significantly below T_C was puzzling.

The measurements on (La, Ca, Pr)MnO$_3$ compounds showed that ferromagnetic CMR compounds develop two Mn-ion spin-lattice relaxation channels as they are cooled below their insulator-metal transition temperature T_{MI}. This result is in contrast to conventional ferromagnets and is attributed to the presence of both insulating and conducting ferromagnetic regions below T_{MI} which coexist on a microscopic scale. The coexistence of different phases is found in both polycrystalline and single-crystalline materials, though the single crystal exhibits a narrower temperature region of phase coexistence below its ferromagnetic critical temperature T_C. The authors discuss possible differences between crystalline and granular materials which could give rise to these findings. These results could have important implications for the use of CMR materials in spintronics devices, which rely on conducting surfaces in thin film multilayers below T_C, where even a thin layer of insulating surface material can degrade performance.

Fatigue crack closure micromechanisms

In situ high resolution synchrotron x-ray tomography of fatigue crack closure micromechanisms

K H Khor, J-Y Buffière, W Ludwig, H Toda, H S Ubhi, P J Gregson and I Sinclair
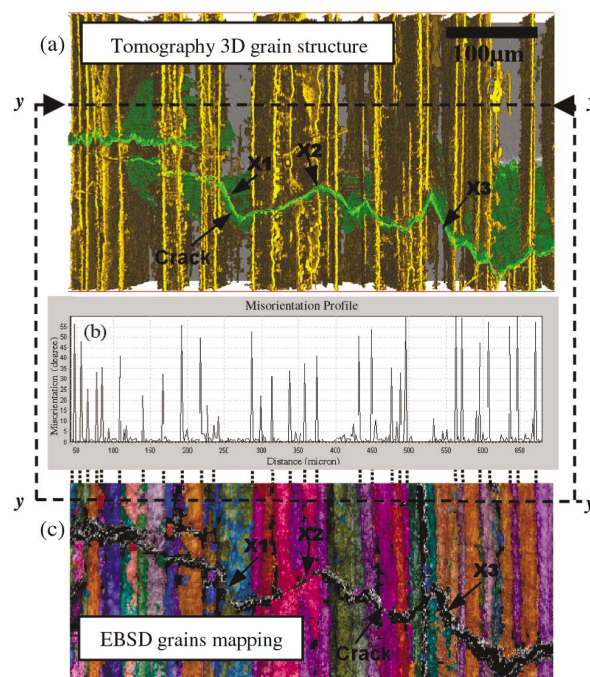
Comparison of the EBSD grains map and tomography data: (a) 3D reconstruction of grain boundaries (yellow) and the crack (green), (b) grain misorientation data from the EBSD data in (c), along the line y-y, and (c) an EBSD orientation map of the sample at the front plane of the image (a).

Fatigue crack closure can have major effects on crack growth rates, but the methods of measuring it are controversial. To date, computed finite-element models, analytical models and widely established compliance-based experimental methods have offered limited micromechanical insight and/or direct information on the active crack tip region within bulk material. To understand the absolute contributions of crack closure mechanisms, such as plasticity-induced and roughness-induced closure, to fatigue properties, an internal, three-dimensional insight into crack behaviour during loading and unloading is clearly of value.

K H Khor (Southampton) and co-workers have carried out synchrotron radiation x-ray microtomography at a high resolution of 0.7 μm to provide unique three-dimensional in situ observation of steady state plane strain fatigue crack growth in a 2024-type Al alloy (Al-Cu-Mg-Mn). Using such high resolution imaging (additionally exploiting the phase contrast effect in interface imaging), the details of fatigue cracks are readily observed, along with the occurrence of closure. They used a novel microstructural crack displacement gauging method to quantify the mixed mode character of crack opening displacement and the closure effect. They observed details of a crack, such as its surface topology, bifurcation and tip geometry, by volume rendering, and obtained evidence of the occurrence and mechanical influence of crack closure. They used a liquid gallium grain boundary wetting technique in conjunction with the microtomography to visualize the correlation between the three-dimensional structure of the grains and fatigue crack behaviour. Subsequently, electron backscattering diffraction assessment of the grain orientation on the samples provided a uniquely complete 3D description of crack-microstructure interactions.

Modelling Charged colloidal suspensions

Fluid particle dynamics simulation of charged colloidal suspensions

Hiroya Kodama, Kimiya Takeshita, Takeaki Araki and Hajime Tanaka
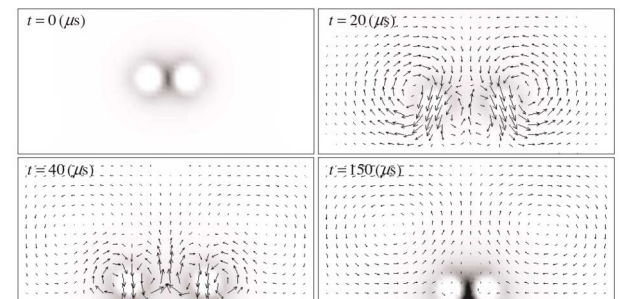
Snapshots of the process of the electrophoretic deposition of two charged particles placed between the electrodes. The density plot represents the counterion concentration. The arrows indicate the velocity field. The electrodes are separated by 310 nm (d = 310 nm). The applied voltage is V = 100 mV. The average concentration of the added salt is 10^{-5} M.

The most difficult problem in studying the dynamics of charged colloidal suspensions arises from the complex dynamic coupling between the motions of the three key elements, namely colloidal particles, ions, and liquid molecules. These elements interact strongly with each other via both electrostatic and hydrodynamic interactions, which are both of long-range nature, so this is a very complex dynamic many-body problem. In most previous studies, the motion of one of these elements has been ignored. This study by Hajime Tanaka's group is the first to take all three components into account.

In principle, molecular dynamics (MD) simulation is a powerful means of studying the dynamic behaviour of charged colloidal suspensions. It incorporates hydrodynamic and electrostatic interactions by explicitly solving for the motions of colloids, ions, and liquid molecules. In reality, however, it is too costly in computer time for dealing with the hydrodynamic motion of liquid molecules and the resulting motion of colloids and ions, so liquid molecules have previously been neglected. The number of colloidal particles and the timescale have to be limited somehow: coarse graining of the problem is essential.

A new simulation method (the fluid particle dynamics (FPD) method) was recently proposed for charge-free colloidal suspensions by Tanaka and Araki. Here liquid molecules are treated as a continuum fluid and a solid colloidal particle is treated as an undeformable fluid of high viscosity. This allows the whole colloidal system to be treated as a continuous liquid with inhomogeneity of the viscosity, which exactly reflects the spatial distribution of colloidal particles.

In the present letter, Tanaka and co-workers present a new simulation method to deal with the dynamics of charged colloidal suspensions while including full hydrodynamic and electrostatic interactions among charged colloidal particles, ion clouds, and liquid. The validity of this method has been demonstrated for the problem of electrophoretic deposition kinetics. The electrostatic and the hydrodynamic interactions as well as the electro-osmotic effect are naturally introduced in the simulation. Although they have shown a two-particle simulation of a small system size in two dimensions, it is quite straightforward for their method to treat a many-particle system and/or a three-dimensional system. The new method should contribute to a deeper understanding of kinetic aspects of complex many-body problems in charged colloidal suspensions.

Wall tensions of colloid-polymer mixtures

Wall tensions of model colloid-polymer mixtures
Paul P F Wessels, Matthias Schmidt and Hartmut Löwen
J. Phys.: Condens. Matter 16 L1-L8
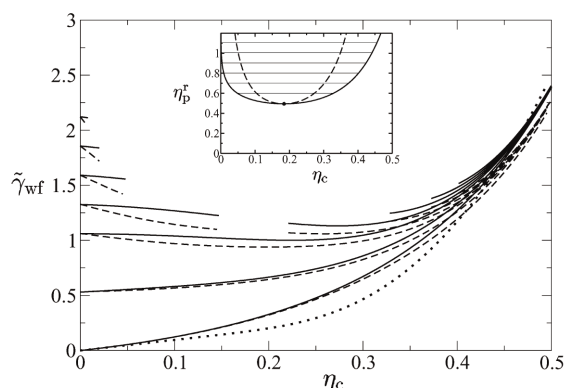
The hard wall-fluid interface tension $\tilde{\gamma}_{wf} = \beta\sigma_c^2 \gamma_{wf}$ of the AO model for size ratio $q = \sigma_p/\sigma_c = 0.6$ as a function of the colloid packing fraction η_c and for increasing polymer reservoir packing fractions $\eta_p' = 0, 0.2, 0.4, 0.5, 0.6, 0.7, 0.8$ (from bottom to top). The results from SPT (full curves) are compared with those of numerical DFT calculations (dashed curves). The gap in the top four curves corresponds to fluid phase coexistence. Also shown is the DFT result for the polymer-coated wall for $\eta_p' = 0.4$ (dotted curve); the corresponding SPT result is equal to γ_{hs} (lowest full curve). The inset shows the fluid part of the phase diagram for $q = 0.6$ as a function of η_c and η_p'; indicated are the binodal (thick curve), spinodal (dotted curve), critical point and (horizontal) tielines connecting coexisting states.

Mixtures of sterically-stabilized colloidal particles and non-adsorbing globular polymers suspended in an organic solvent are valuable soft matter systems to study demixing phase transitions and wetting phenomena at walls. Controlling the wetting behaviour is mandatory for tailoring wall coatings with intriguing applications like self-cleaning surfaces.

The Asakura-Oosawa-Vrij (AO) model of hard sphere colloids and ideal polymer spheres is a widely-used reference system. Hartmut Löwen and co-workers at Düsseldorf and Utrecht present an analytical expression for the wall-fluid tension of the AO model at a hard wall using ideas from scaled particle theory. The key idea is to consider a ternary system of colloids, polymers and a dummy component of large size and vanishing concentration that is equivalent to a planar wall.

They have derived analytical expressions for the wall tension of a colloid-polymer mixture using a scaled particle approach. They considered both the AO model near a hard and a polymer-coated wall (the latter being penetrable for the polymers) and the case of interacting polymers at a hard wall. Their results showed good overall agreement with explicit DFT calculations. Applied to the fluid demixing binodal, their data confirm the wetting transition at the hard wall which has been observed experimentally. The previously found layering transition manifests itself as a tiny kink in the interfacial tension. They predict complete drying near a polymer-coated wall, as has been reported in experiments. Future work could be devoted to exploring the interfacial tensions by direct computer simulation via integrating the anisotropy of the pressure tensor, by thermodynamic integration or, possibly, by using grand-canonical configurational-bias Monte Carlo to test the predictions. It would also be interesting to study patterned surfaces and structured walls, which for example drastically influence the flow through microfluidic devices.

Training effect in CMR manganites

Relationship between the onset of ferromagnetism and the training effect in CMR perovskite manganites
D Zhu, V Hardy, A Maignan and B Raveau
J. Phys.: Condens. Matter 16 L101-L107
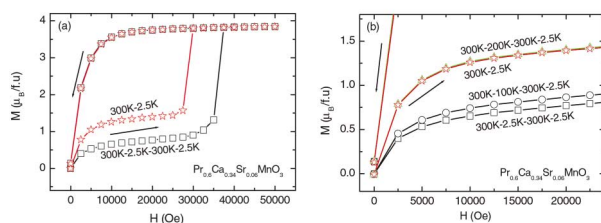
(a) Isothermal M(H) curves of $Pr_{0.6}Ca_{0.34}Sr_{0.06}MnO_3$ registered at $T = 2.5$ K after different thermal cyclings (300 K-2.5 K and 300 K-2.5 K-300 K-2.5 K). (b) The enlargement of the field increasing branches of the M(H) curves after different thermal cyclings. The arrows indicate the magnetic field increasing and decreasing branches.

Mixed-valent perovskite manganites display many extraordinary properties including colossal magnetoresistance and charge ordering. $Pr_{0.5}Ca_{0.5}MnO_3$ exhibits orbital and charge ordering (OO/CO), which corresponds to the 1:1 ratio of $Mn^{3+}:Mn^{4+}$ stripes and is a charge-exchange-type antiferromagnetic insulator (AFMI). This state is very stable, so a high critical field up to 25 T is needed to melt it into a ferromagnetic (FM) state. If the Mn^{3+} content is increased, the OO/CO state is destabilized and the critical field decreases. A decrease of critical field can also be realized by substituting foreign cations at either the A- or B-site, which can lead to the development of FM in the AFM matrix, inducing phase separation.

A Maignan and colleagues at ENSI, Caen have previously performed magnetic-field-driven magnetization measurements on these materials and found that the AFM-FM transition shows abrupt M steps at low temperature. This is not compatible with conventional metamagnetism, while a martensitic-like mechanism was plausible. This interpretation was based on observations such as the training effect, influence of the measuring procedure, recovery of the virgin properties after annealing, role of the microstructure, etc. The existence of phase separation can lead to very peculiar behaviour such as the effect of thermal cycling, which can induce a spectacular increase of resistivity and a change in the $M(H)$ shape. Below the critical field H_1 for the appearance of the first $M(H)$ step, M shifts down and H_1 shifts up as the cycle number increases. This indicates that the FM regions tend to disappear to the benefit of the OO/CO AFM ones, as if the thermal cycling was a 'training' effect for the stabilization of the AFM phase.

In a recent letter Maignan et al report on a precise investigation of this so-called training effect carried out on A-site-substituted perovskite manganites, which allows a fine tuning of the magnetic ground state. Combining ac susceptibility and magnetization measurements during thermal cyclings, they show that the training effect is closely related to the transition from the orbital/charge ordered state to the ferromagnetic metallic state at low temperature, and consequently depends on T_C. They propose that this phenomenon originates from the structural phase separation that appears below T_C, in agreement with the martensitic-like scenario.

Time and length scaling in spin glass dynamics

Time and length scales in spin glasses
L Berthier and A P Young
J.Phys: Condens. Matter 16 S729-S734

The orientation variable $\cos \theta_i(t) = S_i^a(t) \cdot S_i^b(t)$ is encoded in a greyscale in a $60\times60\times60$ simulation box at three different times $t_w = 2, 27,$ and $57\,797$ (from left to right) and temperature $T = 0.04$. The growth of a local random ordering is evident.

The rich dynamical behaviour of spin glasses has been extensively studied in experiments, simulations, and theoretically. In this paper, L Berthier and A P Young discuss the slow, nonequilibrium, dynamics of spin glasses in their glassy phase. Experimental studies of the spin glass phase always probe the nonequilibrium dynamics, because the equilibration time of macroscopic samples is infinite. Simulations can probe equilibrium behaviour for very moderate sizes only, so the thermodynamic nature of the spin glass phase is still a matter of debate. Although many theories account for the simplest experimental results, such as the ageing phenomenon, early experiments revealed several other spectacular phenomena (rejuvenation, memory, etc) that are harder to explain.

Most previous studies have used the Edwards-Anderson model of an Ising spin glass, but very few issues have been settled, notably the existence, for $d \geq 3$, of a second-order phase transition to a spin glass phase. The nonequilibrium dynamics of the Ising spin glass has also been quite extensively studied but, for $d = 3$, some key experimental observations are not reproduced, though simulations in $d = 4$ have been more successful. This may not be too surprising, since real spin glasses are made not of Ising spins but vector spins. When the interaction between spins is isotropic, the system is therefore best described by the Heisenberg spin glass Hamiltonian, treating the spins as three-component vectors of unit length.

Very recent experiments have shown substantial differences between Ising (i.e. very anisotropic) and Heisenberg samples, the nonequilibrium effects being much clearer in Heisenberg samples. Hence, it is hoped that dynamic studies of the Heisenberg spin glass in $d = 3$ will reproduce the key experimental effects, so that deeper theoretical knowledge of the nature of the nonequilibrium dynamics of spin glasses can be gained. This paper presents some preliminary results from the first large-scale numerical simulation of the nonequilibrium dynamics of the three-dimensional Heisenberg spin glass.

The results show that spin variables qualitatively follow the same type of ageing behaviour as in the Ising case, which is due to the slow growth with time of a dynamic coherence length. The observation that very large length scales can be reached in the numerical time window gives us the hope, also confirmed by preliminary work, that the model will allow us to reproduce most of the experimental effects, with the advantage that simulations have direct access to the distributions of length scales involved in phenomenological theories, providing further understanding of spin glass dynamics.

Novel quantum Monte Carlo technique with linear scaling

Linear-scaling quantum Monte Carlo technique with non-orthogonal localized orbitals
D Alfè and M J Gillan
J. Phys.: Condens. Matter 16 L305-L311
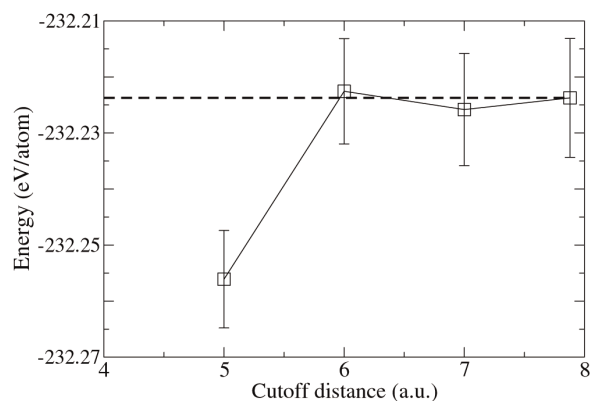
Convergence of linear-scaling diffusion Monte Carlo total energy per atom to the value obtained with extended orbitals for bulk MgO. Open squares with statistical error bars: the present method with cubic cut-off. The dashed line shows the result with extended orbitals. This shows that the energy appears to be converged within ~10 meV/atom for a cut-off radius of 6 au.

Quantum Monte Carlo (QMC) methods, arguably the closest approach to first principles in electronic structure calculations, have now tackled some significant problems in condensed matter. Recent applications include the reconstruction of semiconductor surfaces, the energetics of point defects in insulators, optical excitations in nanostructures, and the energetics of organic molecules. Although its demands on computer power are much greater than those of widely used techniques such as density functional theory (DFT), its accuracy is also much greater for most systems. With QMC now being applied to large complex systems containing hundreds of atoms, a major issue is the scaling of the required computer effort with system size. In other electronic-structure techniques, including DFT, the locality of quantum coherence suggests that it should generally be possible to achieve linear-scaling, or O(N) operation, in which the computer effort is proportional to the number of atoms N. Very recently, a procedure has been suggested by A J Williamson et al for achieving at least partial linear scaling for QMC, based on the idea of 'maximally localized Wannier orbitals' (MLWO).

Here, Dario Alfè and Mike Gillan of University College London propose and test a simpler alternative method, which appears to have important advantages. They have reformulated the QMC technique so that a large part of the calculation scales linearly with the number of atoms. The reformulation is related to MLWO, but has the advantage of greater simplicity. Their technique draws on methods recently developed for linear-scaling density functional theory. They report tests of the new technique on the insulator MgO, and show that its linear-scaling performance is somewhat better than that achieved by the MLWO approach. Implications for the application of QMC to large complex systems are pointed out.

In addition to being simpler and more robust than the earlier technique, the new technique appears also to be more efficient. It makes it possible to treat large systems that would be out of reach of conventional QMC methods. Research areas where the technique is immediately applicable include defects and surfaces of oxide materials, and molecular processes on these surfaces.

Watching diamond form

In situ x-ray diffraction of graphite-diamond transformation using various catalysts under high pressures and high temperatures
Wataru Utsumi, Taku Okada, Takashi Taniguchi, Ken-ichi Funakoshi, Takumi Kikegawa, Nozomu Hamaya and Osamu Shimomura
J. Phys.: Condens. Matter 16 S1017-S1026
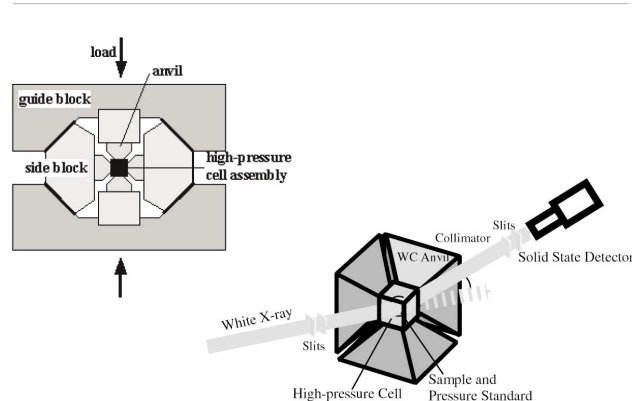
A schematic illustration of the in situ x-ray diffraction system combined with a DIA type multi-anvil high-pressure apparatus.

Synthesis of diamonds using industrial high-pressure technology is now routine, but many questions, such as the role of the catalyst, kinetics of the reaction and the possibility of a metastable phase, remain. The role of inorganic compounds such as carbonates and hydroxides as catalysts for forming diamonds is also of interest. Real-time in situ experiments in which the diamond formation process is directly observed under high pressures and temperatures are indispensable. These experiments are challenging because diamonds are formed in a thick and heavy high-pressure vessel, but are possible using very powerful x-rays from a synchrotron radiation source.

Watari Utsumi at JAIST and co-workers have performed in situ x-ray diffraction studies of graphite-diamond transitions with various solvent catalysts under high pressures and high temperatures at the Photon Factory and SPring-8, which combined synchrotron radiation and a large-volume multi-anvil high-pressure apparatus. They overcame many technical difficulties and made successful real-time observations of the graphite-to-diamond conversion process using various solvent catalysts such as conventional transition metals, carbonate materials and aqueous fluids.

Figure 1 shows a schematic illustration of the *in situ* x-ray diffraction system combined with a DIA type multi-anvil high-pressure apparatus. The incident x-ray beam collimated by the front slits passes through the anvil gap and then irradiates the sample in the high-pressure cell. A typical slit size is 0.05 mm in width × 0.30 mm in height. A pure germanium solid-state detector mounted on a goniometer collected the diffracted x-ray collimated by the receiving slits. The diffraction angle 2θ is fixed at an appropriate value, which is selected for the best diffraction profiles in the region under investigation.

In Utsumi *et al's* paper, the experimental procedure is described and the technical details are explained. The diffraction data with various catalysts are shown and the problems and limitation of this method are discussed.

Phase transitions in Quasi-2D structures

Observation of a semimetal-semiconductor phase transition in the intermetallic ZrTe$_5$
D N McIlroy, S Moore, Daqing Zhang, J Wharton, B Kempton, R Littleton, M Wilson, T M Tritt and C G Olson
J. Phys.: Condens. Matter 16 L359-L365
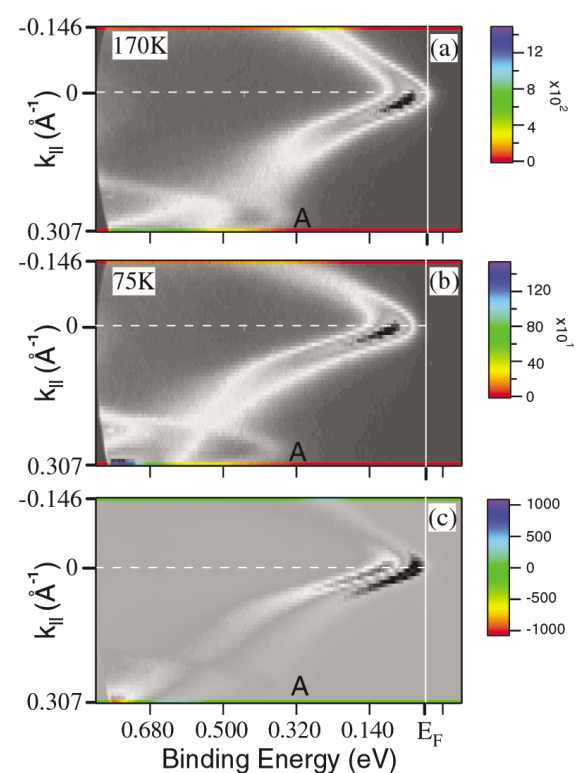
Intensity maps of the density of states of ZrTe$_5$ acquired along the Γ-X high symmetry direction for (a) T = 170 K and (b) T = 75 K, and (c) an intensity difference map between the maps in (a) and (b)

(Quasi)-low-dimensional materials show interesting properties such as superconductivity, colossal magnetoresistance and charge density wave (CDW) formation, typically accompanied by a metal-nonmetal or semimetal-nonmetal transition associated with either the formation of a gap or changes in the width of the gap. Low-dimensional systems are inherently unstable due to correlation and exchange effects, so they exhibit structural instabilities such as Jahn-Teller or CDW distortions.

One class of such materials is the pentatellurides (ZrTe$_5$ and HfTe$_5$), which exhibit anomalous transport properties attributed to their quasi-two-dimensional structure. Their structure consists of zigzag chains of Te atoms along the a-axis that link prismatic chains of ZrTe$_6$ along the c-axis, which together form 2D planes weakly bonded via van der Waals forces along the b-axis. This structure belongs to the *Cmcm* (D_{2h}^{17}) space group.

D N McIlroy of University of Idaho and co-workers used the technique of high-resolution angle-resolved photoelectron spectroscopy to study the temperature dependent electronic structure of ZrTe$_5$. In the temperature range 20-170K they observed a band gap, indicative of a semiconducting phase. In addition, the chemical potential was observed to shift downwards with temperature, consistent with an intrinsic semiconductor. Since ZrTe$_5$ is metallic for $T \leq 4.5$ K, as determined from the Shubnikov-deHaas effect, they concluded that a metal-semiconductor phase transition occurs for 4.2 K < T < 20 K. While they cannot exclude charge density wave formation for T < 20 K, the lack of experimental evidence argues against this explanation for the metal-semiconductor transition. However, their observations suggest that it is a reduction in interplane interactions between the a-c planes of ZrTe$_5$ that is responsible for the transition.

A thorough study of the temperature dependent phonon density of states is needed to shed light on the origin of the phase transition.
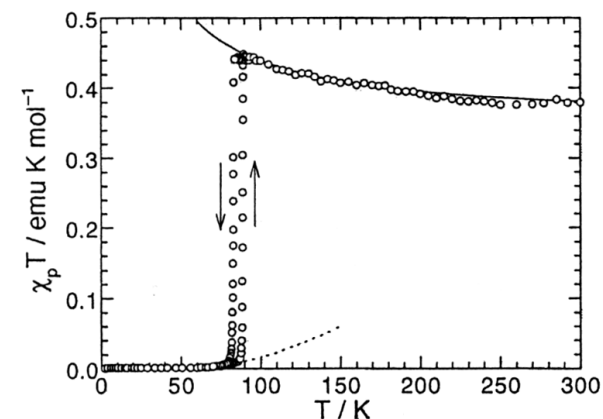
TOPICAL REVIEWS AND SPECIAL ISSUE PAPERS

Organic and molecular magnets

Organic and molecular magnets
S J Blundell and F L Pratt
J. Phys.: Condens. Matter 16 R771-R828

The magnetic susceptibility of galvinoxyl. Ferromagnetic interactions dominate above the phase transition at 85 K. The high-temperature behaviour fits to a one-dimensional ferromagnetic Heisenberg model and the low-temperature behaviour fits to a singlet-triplet model.

Though magnetism is traditionally associated with metals or simple compounds, some of the most exciting recent studies in magnetism are on organic materials. Organic and molecular materials have an extraordinarily diverse range of magnetic properties. The use of organic and molecular building blocks can lead to new magnetic materials with intriguing properties which have, on occasion, led to the discovery of new physics. Stephen Blundell (Oxford) and Francis Pratt (Rutherford Appleton Laboratory) review this rapidly emerging field.

Purely organic ferromagnets, based upon nitronyl nitroxide radicals, show long-range magnetic order at very low temperatures in the region of 1 K, while sulfur-based radicals show weak ferromagnetism at temperatures up to 36 K. It is also possible to prepare molecule-based magnets in which transition metal ions are used to provide the magnetic moment, but organic groups mediate the interactions. This strategy has produced magnetic materials with a large variety of structures, including chains, layered systems and three-dimensional networks, some of which show ordering at room temperature and some of which have very high coercivity. Even if long-range magnetic order is not achieved, the spin crossover effect may be observed, which has important applications. Further magnetic materials may be obtained by constructing charge transfer salts, which can produce metallic molecular magnets. Another development is single-molecule magnets, formed by preparing small magnetic clusters. These materials can show macroscopic quantum tunnelling of the magnetization and may have uses as memory devices or in quantum computation applications.

The search is currently on for new materials with higher coercivities, higher transition temperatures, more pronounced anisotropies, or larger magnetoresistance. Many puzzles remain to be solved in, for example, the behaviour of single-molecule magnets and the relationship between magnetism and superconductivity. Moreover, little has so far been done to understand how domains behave in organic and molecular magnets. The advances already gained in this field have originated through developments in synthetic and coordination chemistry, but the whole enterprise is an interdisciplinary effort, involving both physicists and chemists, which promises to remain fast moving and continually surprising.

Coarse grain simulation of soft matter

Coarse grain models and the computer simulation of soft materials
Steve O Nielsen, Carlos F Lopez, Goundla Srinivas and Michael L Klein
J. Phys.: Condens. Matter 16 R481-R512
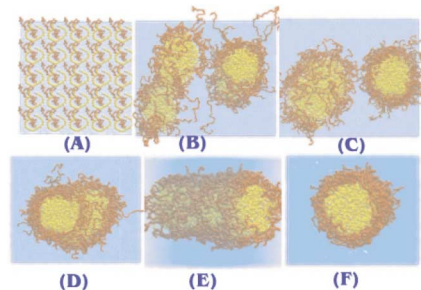
Self-assembly of a worm-like micelle as observed in CG simulations. Simulations are started from a lattice configuration (A) with 100 $EO_{40}EE_{37}$ diblock copolymers in 20 000 CG water sites. Aggregation of the hydrophobic blocks into two clusters (B), (C) is followed by their merger (d) into a worm-like micelle which spans the simulation unit cell, shown from two viewpoints (E), (F). The EO monomers are shaded dark; the light EE monomers form the core of the micelle.

Experimental work on complex condensed matter spans a broad range of temporal and spatial scales, from femtosecond dynamics and atomistic detail to real-time macroscopic phenomena. Simulation methods in which each atom is explicitly represented are well established but have difficulty addressing many cooperative effects of experimental and theoretical interest. Bridging the disparate time and spatial scales is possible with multiscale modeling, in which the various levels of treatment are coupled and fed back into one another.

Michael Klein and colleagues from University of Pennsylvania review a coarse grain (CG) simulation method that has ready access to events on these scales. They give some illustrative examples from biology and materials science and they summarise existing simulation techniques which access intermediate timescales and length scales. They provide insights into the model building process and discuss consequences arising from the loss of detail. They look at a few situations in which theoretical predictions can be evaluated by CG simulation methods, and at several situations in which the CG method goes beyond current theoretical and experimental reach. Finally they give some perspectives on future directions for research using CG models.

Many topics are amenable to study with the CG method. Bilayers and monolayers involving a few lipid species and cholesterol are suitable for studying raft formation. The compression/expansion cycle of the lung surfactant DPPC could be studied in the presence of the surfactant proteins (SPs), which are known to alter monolayer collapse. Lipid mediated protein-protein interactions can be used to explore membrane protein crystallization. The cyclic D,L-α-peptide nanotubes of Ghadiri *et al* could be studied for their self-assembly and membrane disruption properties. Monolayer structure at solid/water interfaces displays novel geometry such as hemicylindrical micelles which is being elucidated with atomic force microscopy. Entropic and enthalpic interactions between amphiphile surfaces such as micelles, lipid bilayers, microemulsion droplets, and combinations thereof can be computed as potentials of mean force. Protein alignment can be studied as a function of surface pressure in Langmuir monolayers. Self-assembled vesicles from non-lipid species such as surfactant-like peptides or block copolymers offer alternatives for many applications including targeted drug delivery. In conclusion, there are clearly many possible future applications of CG models.

Simple models of protein folding

Simple models of protein folding and of non-conventional drug design
R A Broglia, G Tiana and D Provasi
J. Phys.: Condens. Matter 16 R111-R144
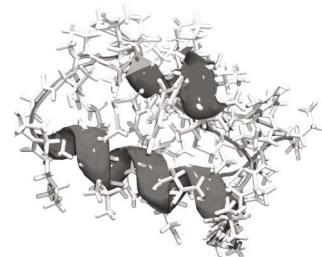
The atomic structure of a small protein, Chemotrypsin Inhibitor 2. The dark grey curve highlights the chain structure.

The protein folding problem, one of the great unsolved problems of science, is simply stated: how does the one-dimensional structure of a protein (a sequence of amino acids) determine the three-dimensional structure into which it folds? An even more elusive goal is the prediction of the catalytic activity of an enzyme from its amino acid sequence. This is the subject of a review by G Tiana and colleagues from Milan.

While all the information required for the folding of a protein is contained in its amino acid sequence, it is not yet known how to extract this information to predict the three-dimensional, biologically active, native conformation of a protein from its sequence. Using insights obtained from simple model simulations of the folding of proteins, in particular the fact that this phenomenon is essentially controlled by conserved (native) contacts among (few) strongly interacting ('hot'), as a rule hydrophobic, amino acids, which also stabilize local elementary structures (LES, hidden, incipient secondary structures such as _-helices and _-sheets) formed early in the folding process and leading to the postcritical folding nucleus (i.e. the minimum set of native contacts which brings the system beyond the highest free-energy barrier found in the whole folding process) it is possible to work out a successful strategy for reading the native structure of designed proteins from a knowledge of only their amino acid sequence and of the contact energies among the amino acids. Because LES have undergone millions of years of evolution to selectively dock to their complementary structures, small peptides made out of the same amino acids as the LES are expected to selectively attach to the newly expressed (unfolded) protein and inhibit its folding, or to the native (fluctuating) native conformation and denature it. These peptides, or their mimetic molecules, can thus be used as effective non-conventional drugs to those already existing (and directed at neutralizing the active site of enzymes), displaying the advantage of not suffering from the increase in resistance.

See also a recent review by F Galisteo-González (Granada) and co-authors.

Measurement of interactions between protein layers adsorbed on silica by atomic force microscopy
J J Valle-Delgado, J A Molina-Bolívar, F Galisteo-González, M J Gálvez-Ruiz, A Feiler and M W Rutland
J. Phys.: Condens. Matter 16 S2383-S2392

Using an atomic force microscope and the colloid probe technique, they investigated the interaction forces between bovine serum albumin (BSA) layers and between apoferritin layers adsorbed on silica surfaces.
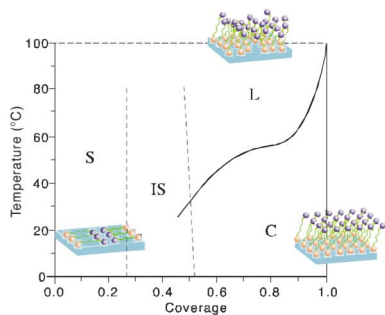
The measurements were carried out in an aqueous medium at different pH values and NaCl concentrations.

Self-assembled monolayers

Self-assembled monolayers: from 'simple' model systems to biofunctionalized interfaces
Frank Schreiber
J. Phys.: Condens. Matter 16 R881-R900

Schematic phase diagram of decanethiol on Au(111) in temperature and coverage space. The different regions and phases are denoted as S (stripes), IS (intermediate structures), C (c(4×2)), and L (liquid). The broken lines indicate phase boundaries of the IS, which are not yet fully established. The solid curve between C and L (melting transition) exhibits a sharp rise near full coverage. Note that this is similar to the behaviour found for much simpler systems such as nitrogen on graphite

Frank Schreiber (Oxford) reviews recent developments in the area of self-assembled monolayers (SAMs) and their applications. There is increasing interest in soft condensed matter, and in thin films additional issues related to the reduced dimensionality come into play.

The term 'self-assembly' may be defined as the spontaneous formation of complex hierarchical structures from pre-designed building blocks, typically involving multiple energy scales and multiple degrees of freedom. Specifically, self-assembled monolayers are ordered molecular assemblies that are formed spontaneously by the adsorption of a surfactant with a specific affinity of its headgroup to a substrate. They are usually prepared from solution, although some systems can be prepared from the vapour as well.

The discovery of SAMs has transformed surface chemistry and also led to new physics. It has brought together the study of well defined inorganic surfaces and organic species, which from a physics perspective were previously often considered rather undefined. The great flexibility of the concept of SAMs brought about by the wide choice of endgroups which can be anchored to the substrate has led to a broad range of applications of SAMs including important developments in the area of biotechnology.

Schreiber first discusses issues related to the structure, the phase transitions, the phase diagram, and the growth dynamics. He explains how the internal degrees of freedom and the multiple interactions involved can lead to fairly rich phase behaviour even for systems which are commonly considered 'simple' model systems. Then he discusses selected problems for more complex SAM-based systems, including SAMs as substrates for growth, SAMs and molecular electronics, electrochemical applications, and 'switchable' SAMs, as well as the use of SAMs for biofunctionalized surfaces and lateral structuring.

The fundamental questions of adsorption, structure, phases, and phase transitions have been thoroughly studied in the past, but several issues remain unresolved, probably reflecting the complex competition of multiple interactions and degrees of freedom, giving rise to various structures which are energetically similar. Much present and future work is related to utilizing the various ways to modify and functionalize surfaces by SAMs, with biorelated applications being the most dynamic area. Since SAMs are not so much a specific class of compounds, but rather a very flexible concept with virtually unlimited potential for applications, we expect that the area of SAMs will continue to thrive.

Quantum cascade structures

Coherent charge transport in semiconductor quantum cascade structures
Michael Woerner, Klaus Reimann and Thomas Elsaesser
J. Phys.: Condens. Matter 16 R25-R48
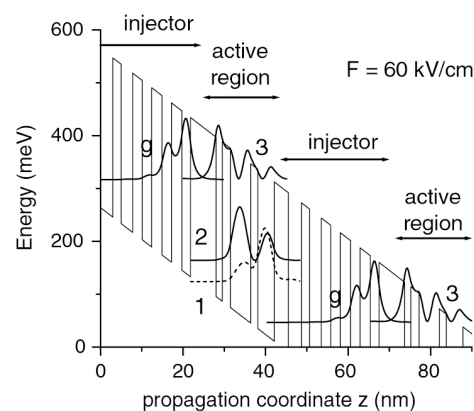
A conduction band diagram of the $GaAs/Al_{0.33}Ga_{0.67}As$ quantum cascade laser structure (sample A). Probability densities $|\psi(z)|^2$ are shown for the wavefunctions relevant for the QCL dynamics: $|g\rangle$ (ground state in the injector), $|3\rangle$ (upper laser state), $|2\rangle$ (lower laser state) and $|1\rangle$ are eigenstates of the electronic Hamiltonian without the tunnel coupling through the injection barrier (the wide barrier to the left of the active region).

Quantum cascade structures have wide application in electrically driven semiconductor lasers working in the mid- to far-infrared spectral range. Optical amplification in such unipolar devices is based on a population inversion between quasi-two-dimensional conduction subbands in coupled quantum wells. The population inversion in the active region is generated by electrons tunnelling from an injector region through a barrier into the upper laser subband and by ultrafast extraction of these electrons out of the lower laser subband through a barrier into the next injector region. Such transport processes on ultrafast timescales have been the subject of extensive experimental and theoretical work without reaching a clear physical picture of the microscopic electron dynamics.

Thomas Elsaesser of the Max Born Institut and colleagues review a comprehensive experimental study of electron transport in electrically driven quantum cascade structures. They investigated ultrafast quantum transport from the injector into the upper laser subband by mid-infrared pump-probe experiments directly monitoring the femtosecond saturation and subsequent recovery of electrically induced optical gain. For low current densities, low lattice temperatures and low pump pulse intensities, the charge transport is dominantly coherent, leading to pronounced gain oscillations due to the coherent motion of electron wavepackets. For higher current densities, lattice temperatures, or pump intensities, the gain recovery shows an additional incoherent component, which essentially follows the pump-induced heating and subsequent cooling of the carrier gas in the injector.

Even at the high electron densities present in a quantum cascade laser the coherence properties of the electron wavefunction play an important role for the microscopic injection process. This process is crucial for generating gain in quantum cascade lasers and represents a key step in the overall charge transport through the device. These results strongly support the empirical finding that the design of the wavefunction overlap between the injector subbands and the upper laser subband is essential for the performance of a quantum cascade laser. Theoretical calculations that include both the quantum character of transport and the decoherence caused by electron-electron scattering are still lacking and pose a challenge for the future.

Slow and fast light in solids

Ultra-slow and superluminal light propagation in solids at room temperature
M S Bigelow, N N Lepeshkin and R W Boyd
J. Phys.: Condens. Matter 16 R1321-R1340
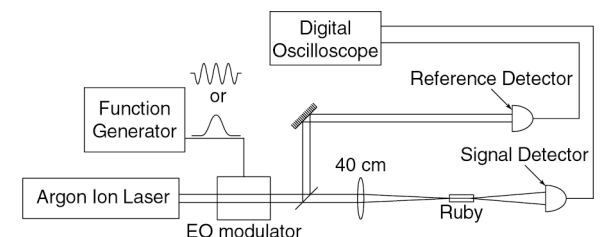
The experimental setup used to observe slow light in ruby.

Recent interest in the old problem of how a wave travels through a dispersive material has been sparked by the discovery of systems that have high dispersion, yet allow a pulse to propagate relatively undistorted. In addition, these new systems have relatively low loss so the pulse dynamics are easy to observe. However, until now, all of the systems developed to generate slow or fast light have been difficult to implement.

In this review, R W Boyd and colleagues at Rochester University explore ways to produce slow and fast light in a room-temperature solid-state material. First they describe the concept of coherent population oscillations—the primary physical mechanism used to generate large dispersion. They show that when the beat frequency between the pump and probe beams is slow enough, it will cause the population in a two-level atom to oscillate. This time-varying population will cause energy to be scattered out of the pump beam and into the probe, so the probe will see less absorption over a narrow frequency range. Correspondingly, the group velocity for the probe can be very large within the same frequency range.

They describe their experimental demonstration of ultra-slow light propagation in ruby using coherent population oscillations. They observed a group velocity as low as 58 m s^{-1}. Their results included the observation of a delay of both amplitude modulations and pulses.

They showed how it is possible to observe both ultra-slow and superluminal group velocities in another material, alexandrite. Since alexandrite is an inverse saturable absorber at certain wavelengths, the sign of the group velocity is changed. In alexandrite the chromium ions can occupy either mirror sites (having mirror symmetry) or inversion sites (having inversion symmetry). As a result of the energy level structure at each site, ions at mirror sites experience inverse-saturable absorption (fast light), whereas ions at inversion sites experience saturable absorption (slow light). The competing effects from ions at either site can be easily distinguished because they have markedly different population relaxation times.

Finally, the authors discuss the significance of ultra-slow light propagation. While much work remains to be done, they conclude that these slow light techniques could be very important in developing all-optical control of communication and storage applications.

Read-out of single spins

Read-out of single spins by optical spectroscopy
F Jelezko and J Wrachtrup
J. Phys.: Condens. Matter 16 R1089-R1104
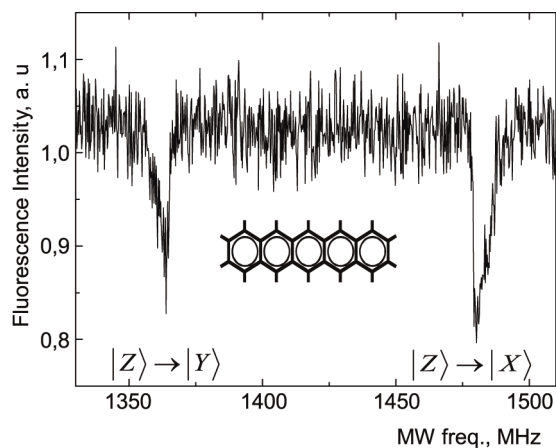
The ODMR spectrum of a single pentacene molecule. The inset shows the chemical structure of pentacene.

Quantum computing is tantalising. It exploits the idea that a quantum mechanical system can exist in a superposition of several states at once, so it might be used for parallel data processing, enabling an exponential speed-up of certain calculations. The opportunities are driving a growing interest in manipulation and read-out of single-electron and nuclear spin states because of possible applications in solid state quantum computing.

F Jelezko and J Wrachtrup of University of Stuttgart review recent experiments on optical detection and manipulation of spin states of impurity centres in a solid. They introduce the experimental background of optical detection of single quantum systems in solids. The interaction of an impurity centre with an excitation field is analysed in terms of optical Bloch equations. They present recent experiments on the electron spin resonance of single organic molecules and paramagnetic defect centres in diamonds and they show how the spin state of the nitrogen-vacancy paramagnetic defect in diamond can be read out optically. They also discuss pulsed electron spin resonance of the single paramagnetic defect centre in diamond.
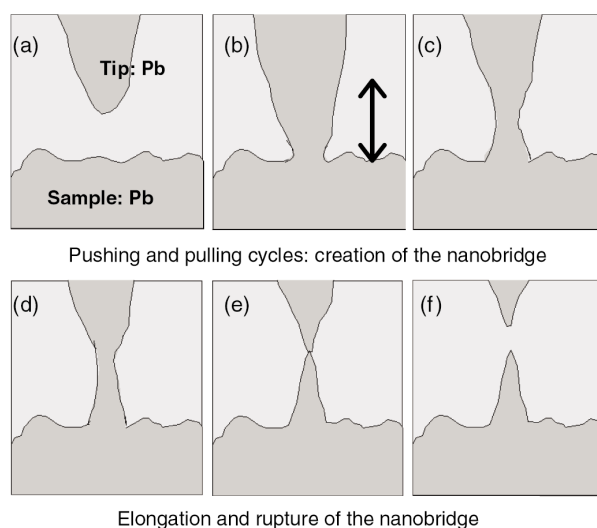
The accurate measurement of a single spin state has two important aspects. First, single-spin magnetic resonance is a central point for any pure state based quantum computing scheme. Several promising techniques are currently under investigation. Recently, controlled electron spin injection and single-spin detection were demonstrated using electrical read-out in quantum dots and scanning tunnelling microscopy of organic molecules. Important progress has been achieved in the field of magnetic resonance force microscopy, which recently showed detection sensitivity of two electron spins. Yet optical detection remains a unique technique, capable of demonstrating coherent ESR and NMR in experiments on single quantum systems. The next step will be to show coupling between several spins. This will allow achievement of two-qubit gates, which are basic elements for quantum computing. The second important field is of more fundamental character. Experiments with single spins are suitable for experimental testing of quantum mechanics. Projective spin measurements on single quantum systems can be used in tests of the quantum Zeno effect and Bell's inequalities.

Superconducting nanostructures

Superconducting nanostructures fabricated with the scanning tunnelling microscope
J G Rodrigo, H Suderow, S Vieira, E Bascones and F Guinea
J. Phys.: Condens. Matter 16 R1151-R1182

Pushing and pulling cycles: creation of the nanobridge

Elongation and rupture of the nanobridge

Sketch of the nanobridge fabrication process. Frames (a)-(f) illustrate different stages of the process: (a) tip and sample in tunnelling regime; (b) the tip is pressed against the substrate, both electrodes deform plastically and forma connective neck; (c)-(e) indentation-retraction cycles produce a plastic elongation of the neck; (f) the rupture of the nanobridge takes place.

Low-dimensional conducting and superconductor systems reveal much new physics, as is evident from reports of experiments with single small particles, thin wires, carbon nanotubes or DNA molecules. Control of the nanoworld has been revolutionized by the invention of the scanning tunnelling microscope (STM) and related techniques such as atomic force microscopy, magnetic force microscopy and scanning Hall probe microscopy.

S Vieira (Madrid and co-workers review the properties of nanoscopic superconducting structures fabricated with a scanning tunnelling microscope, with emphasis on the effects of high magnetic fields. These systems include the smallest superconducting junctions which can be fabricated, and they are a unique laboratory in which to study superconductivity under extreme conditions. The review covers a variety of recent experimental results on these systems, highlighting their unusual transport properties, and theoretical models developed for their understanding.

Charge transport through superconducting nanobridges can be dramatically modified by small changes in the minimal cross-section region, the neck, but the overall nanostructure (nanobridge) remains unmodified when scanning through these regimes. At a high level of current, heating and other nonequilibrium effects appear. In atomic-size contacts superconductivity and quantum transport phenomena can be studied in a well controlled manner. Breaking the tip into two parts results into two atomic size nanotips. One of these can be in situ transported elsewhere and used to perform atomic resolution microscopy and spectroscopy over a sample, without change in vacuum or temperature conditions. The application of an external magnetic field confines the condensate around the bridge region, creating a nanoscopic superconductor with a perfect interface with the normal region, solving in a natural way the contacting problems associated with this kind of structure. This unique system gives us the possibility to perform experiments in a highly controlled situation. Theoretical calculations using Ginzburg-Landau theory and Usadel equations provide a framework to understand the most important aspects of superconductivity in these bridges.